Near DC force measurement using PVDF sensors

Arun Kumar Ramanathan, Leon M. Headings, Marcelo J. Dapino

Arun Kumar Ramanathan, Leon M. Headings, Marcelo J. Dapino, "Near DC force measurement using PVDF sensors," Proc. SPIE 10602, Smart Structures and NDE for Industry 4.0, 106020M (27 March 2018); doi: 10.1117/12.2296849

SPIE.

Event: SPIE Smart Structures and Materials + Nondestructive Evaluation and Health Monitoring, 2018, Denver, Colorado, United States

Near DC force measurement using PVDF sensors

Arun Kumar Ramanathan, Leon M. Headings and Marcelo J. Dapino*

NSF IUCRC on Smart Vehicle Concepts, Department of Mechanical and Aerospace Engineering
The Ohio State University, Columbus, OH 43210

ABSTRACT

There is a need for high-performance force sensors capable of operating at frequencies near DC while producing a minimal mass penalty. Example application areas include steering wheel sensors, powertrain torque sensors, robotic arms, and minimally invasive surgery. The beta crystallographic phase polyvinylidene fluoride (PVDF) films are suitable for this purpose owing to their large piezoelectric constant. Unlike conventional capacitive sensors, beta crystallographic phase PVDF films exhibit a broad linear range and can potentially be designed to operate without complex electronics or signal processing. A fundamental challenge that prevents the implementation of PVDF in certain high-performance applications is their inability to measure static signals, which results from their first-order electrical impedance. Charge readout algorithms have been implemented which address this issue only partially, as they often require integration of the output signal to obtain the applied force profile, resulting in signal drift and signal processing complexities. In this paper, we propose a straightforward real time drift compensation strategy that is applicable to high output impedance PVDF films. This strategy makes it possible to utilize long sample times with a minimal loss of accuracy; our measurements show that the static output remains within 5% of the original value during half-hour measurements. The sensitivity and full-scale range are shown to be determined by the feedback capacitance of the charge amplifier. A linear model of the PVDF sensor system is developed and validated against experimental measurements, along with benchmark tests against a commercial load cell.

Keywords: piezoelectric, PVDF sensor, quasi-static, charge amplification, drift compensation, force-voltage model

1. INTRODUCTION

There is a need for low profile, low cost, and high-performance force sensors for a range of applications from dexterous manipulation with robots to powertrain torque measurements. Conventional force sensors and load cells based on piezoresistive sensors tend to be massive and often require elaborate signal processing circuitry in order to perform direct force measurements. They also tend to become expensive with higher sensitivity and bandwidth requirements. Piezoelectric materials, on the other hand, have been extensively used in this area for their superior noise immunity, high sensitivity, and relatively low cost. The advent of thick-film technology has further facilitated embedment of the sensors for real-time structural health monitoring applications[1].

Polyvinylidene fluoride (PVDF) is a flexible, low density polymer manufactured as thin sheets and thus conformable to arbitrarily shaped structures. When crystallized into its beta phase, PVDF exhibits piezoelectric properties, generating electrical charge in response to an applied stress and vice versa. Due to their high piezoelectric constant and possibility to operate without complicated circuitry, they are strong candidates for many sensing applications. When PVDF is bonded to a structure, it generates charge proportional to the stress transferred to it by the host structure. However, when the applied stress input is static or nearly static, the measurement signal produced by the film decays exponentially. This has largely limited their usage to dynamic sensing applications, such as strain rate measurement[2,3], structural health monitoring[4], detection of shock pulse[5], wave propagation measurements[6], and microphones[7].

*Further author information: (Send correspondence to M.J.D.)
M.J.D.: E-mail: dapino.1@osu.edu
A.K.R.: E-mail: ramanathan.38@osu.edu
L.M.H.: E-mail: headings.4@osu.edu

Smart Structures and NDE for Industry 4.0, edited by Norbert G. Meyendorf, Dan J. Clingman, Proc. of SPIE Vol. 10602, 106020M · © 2018 SPIE · CCC code: 0277-786X/18/$18 · doi: 10.1117/12.2296849

Models for voltage output and sensitivity of PVDF sensors have been developed and validated for strain rate measurements[1], but their applicability to static force measurements have not been reported in the literature. Several techniques have been proposed in the literature to improve their response in low frequency measurements. These techniques can be broadly classified into two types: resonator type and charge integration type.

The resonator type static force measurement technique can be further classified into stand-alone type and excitation-detection type. Stand-alone resonators[8-10] are structures with only one piezoelectric layer actuated by a sinusoidal voltage near its resonance frequency. The applied stress will shift the resonance frequency and can be computed from the variation of the resonance frequency. Excitation-detection type resonators[11-13] consist of two piezoelectric layers. One of the piezoelectric layers will actuate the structure near its resonance frequency and the other will detect the voltage from the resulting vibration of the structure. The difference between the actuation voltage and the detection voltage from the resultant vibration is then used to compute the applied load. A resonator type measurement can only measure the static component of the input signal and a separate sensing system[14] is often required to measure the dynamic component. Lin et al.[15] demonstrated an excitation-detection type resonator that monitors the change in electrical admittance, thereby facilitating measurement of both static and dynamic signals. However, resonator type measurements suffer from high voltage requirements for actuation and expensive signal processing circuitry for direct readout of the applied force.

Direct integration of the charge output from a piezoelectric sensor is implemented using a charge amplifier. Due to the finite first-order output impedance of a PVDF sensor ($>10^{12}\ \Omega$), the generated charge decays with time. However, charge amplifiers have greatly increased the number of practical applications of piezoelectric sensors, particularly in low frequency measurements. But their applicability to near DC applications creates a number of implementation issues. The most important issue is drift in the measured voltage due to the input bias current of the operational amplifier. Lord et al.[16] estimated the drift voltage associated with feedback capacitance for a given operational amplifier and externally compensated for the error in the output voltage of a PZT load cell. Park et al.[17] developed a charge readout algorithm based on electronic systems to improve the force response in low frequency measurements. The technique uses periodic resetting of the feedback capacitor and digitally integrating the output signal from the charge amplifier. This implementation is now available commercially as an IVC102 operational amplifier and the integrated signal is known to be associated with measurement error due to the periodic resetting operation. In addition, this algorithm has a "blind" phase, i.e. an interval when changes in the input signal are not measured. Brandolini et al.[18] proposed a modified circuit in order to counter these disadvantages. However, the proposed circuit was followed by digital integration of the charge output, thus placing a hard limit on the upper cutoff frequency of the system. Rosenbaum et al.[19] developed a low-cost force sensor for quasi static measurements using a state estimation machine, which continuously estimated the bias current from the operational amplifier and supplied a compensating current, followed by a digital integration of the output from the charge amplifier. Nonetheless, the implementation involves sophisticated circuitry of digital implementation. To the best of our knowledge, a robust analog implementation for direct readout of near DC force input is not available.

In this article, we demonstrate an analog drift compensation technique for near DC force measurements implemented around a commercial PVDF sensor. The chief objectives of this work are:

1. Develop a system-based model for the piezoelectric force sensor system;
2. Demonstrate the linearity and fidelity of the proposed drift compensation technique for long sample time measurements; and
3. Experimentally validate the model's sensitivity and response to step inputs.

In addition to their piezoelectricity, PVDF sensors also exhibit pyroelectricity, i.e., they generate charge due to changes in temperature. Temperature cross-sensitivity of PVDF is outside the scope of this current work. Therefore, in both model development and experiments, the temperature is assumed to be constant at 25°C.

2. SYSTEM-BASED APPROACH TOWARDS NEAR DC FORCE MEASUREMENT

The output voltage from a piezoelectric PVDF film attached to a structure in response to an input force can be modeled as a second order mechanical system cascaded together with a first order electrical system[3]. Consider a piezoelectric film of length l_s, width w_s, and thickness t_s bonded to a host structure of length l_b, width w_b, and thickness t_b symmetric about the center of the beam. A schematic of the PVDF force sensing system is shown in Figure 1(a). Assuming no externally applied electric field and negligible stiffness of the PVDF film, the block diagram of the sensing system can be represented as in Figure 1(b).

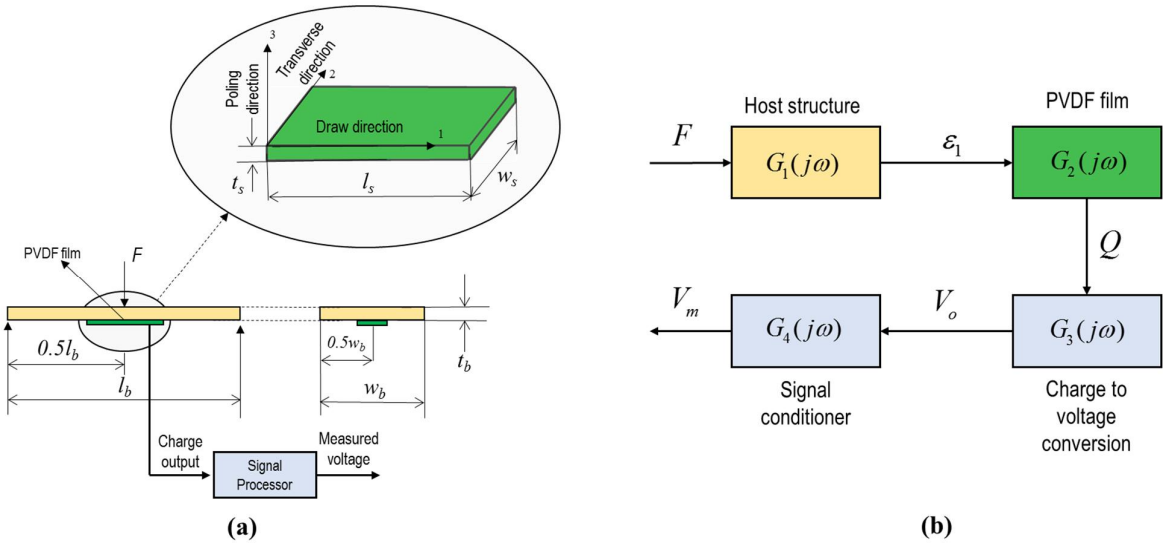

Figure 1. (a) Schematic of the PVDF sensor, (b) block diagram of the PVDF sensor system.

2.1. Force – strain transfer function

The transfer function of a single degree-of-freedom second-order mechanical system, $G_1(j\omega)$, relates the force input $F(j\omega)$ to the induced longitudinal strain in the PVDF film $\varepsilon_1(j\omega)$ as

$$G_1(j\omega) = \frac{\varepsilon_1(j\omega)}{F(j\omega)} = \frac{S_C}{\left(\frac{-\omega^2}{\omega_n^2} + j\frac{2\zeta\omega}{\omega_n^2} + 1\right)};\ s = j\omega \tag{1}$$

where ω is the excitation frequency, ω_n is the natural frequency, ζ is the relative damping, and S_C is the static compliance of the second order mechanical system. For example, assuming pure bending of the simply supported host structure subjected to a midpoint load, S_C can be given by

$$S_C = \frac{3l_b}{2E_b w_b t_b^2}. \tag{2}$$

A single degree-of-freedom approximation of the mechanical system may not be possible for complicated structures. However, for systems involving excitation frequencies much lower than their fundamental frequency, such approximations can be identified by computing their vibration modes using the finite element method.

2.2. Strain – charge transfer function

Piezoelectric materials act as sensors by generating electrical charge in proportion to the applied stress or act as actuators by generating strain in response to an applied electric field. The linear coupled constitutive relationship for a piezoelectric material in strain-charge form is given as[7]

$$\begin{aligned} \varepsilon_p &= s_{pq}^{E,\theta} T_q + d_{kp}^{\theta} E_k + \alpha_p^E \Delta\theta \\ D_i &= d_{iq}^{\theta} T_q + K_{ik}^{T,\theta} E_k + p_i^T \Delta\theta \end{aligned} \tag{3}$$

where T, E, and θ are independent variables and the superscripts indicate that the quantities are kept constant during their measurement. The tensor notations i and k take values from 1 to 3, while the compressed tensor notations p and q take values from 1 to 6. Figure 1(a) shows the axes corresponding to the above notations.

The representations of the symbols in (3) are as follows:

ε_p	strain tensor
s_{pq}	compliance tensor
T_q	stress tensor
E_i	electric field
$\Delta\theta$	change in temperature
D_i	electric displacement
d_{iq}	piezoelectric charge constant
K_{ik}	permittivity tensor
α_p	thermal coefficient of expansion
p_i	pyroelectric coefficient

If the temperature is kept constant during measurements and if there is no externally applied electric field, i.e. $\Delta\theta = 0$ and E_i=0, then the piezoelectric constitutive equations are decoupled in the strain-charge form. The strain field and electric displacement in the piezoelectric film from equation (3) then reduce to

$$\begin{aligned} \varepsilon_p &= s_{pq} T_q \\ D_i &= d_{iq} T_q . \end{aligned} \tag{4}$$

Note that the superscripts on s_{pq} and d_{iq} are dropped in further analysis for brevity, but their meaning do not change.

The tensor forms of the piezoelectric moduli d_{iq} and the compliance s_{pq} depend on the individual crystal class. For PVDF, a symmetry of type C_{2v} exists and the corresponding d_{iq} and s_{pq} matrices are given by

$$d = \begin{bmatrix} 0 & 0 & 0 & 0 & d_{15} & 0 \\ 0 & 0 & 0 & d_{24} & 0 & 0 \\ d_{31} & d_{32} & d_{33} & 0 & 0 & 0 \end{bmatrix}, \qquad s = \begin{bmatrix} s_{11} & s_{12} & s_{13} & 0 & 0 & 0 \\ s_{12} & s_{22} & s_{23} & 0 & 0 & 0 \\ s_{13} & s_{23} & s_{33} & 0 & 0 & 0 \\ 0 & 0 & 0 & s_{44} & 0 & 0 \\ 0 & 0 & 0 & 0 & s_{55} & 0 \\ 0 & 0 & 0 & 0 & 0 & s_{66} \end{bmatrix}.$$

Electric displacement in equation (4) can now be represented in matrix form as

$$\begin{bmatrix} D_1 \\ D_2 \\ D_3 \end{bmatrix} = \begin{bmatrix} 0 & 0 & 0 & 0 & d_{15} & 0 \\ 0 & 0 & 0 & d_{24} & 0 & 0 \\ d_{31} & d_{32} & d_{33} & 0 & 0 & 0 \end{bmatrix} \begin{bmatrix} T_1 \\ T_2 \\ T_3 \\ T_4 \\ T_5 \\ T_6 \end{bmatrix}. \tag{5}$$

Since the poling of the piezoelectric film is in direction 3, equation (5) can be reduced to

$$D_3 = d_{31}T_1 + d_{32}T_2 + d_{33}T_3. \tag{6}$$

For the film used in a plane stress configuration and assuming there is no shear lag effect due to the thickness of the bond layer, equation (6) can be reduced to

$$D_3 = d_{31}T_1 + d_{32}T_2. \tag{7}$$

Furthermore, using equation (4) a simplified linear stress-strain relationship for the in-plane strains can be obtained as

$$\begin{aligned} \varepsilon_1 &= s_{11}T_1 + s_{12}T_2 \\ \varepsilon_2 &= s_{12}T_1 + s_{22}T_2. \end{aligned} \tag{8}$$

Now solving for the in-plane stresses in equation (8), one obtains

$$\begin{aligned} T_1 &= \frac{s_{22}}{s_{11}s_{22} - s_{12}^2}\varepsilon_1 - \frac{s_{12}}{s_{11}s_{22} - s_{12}^2}\varepsilon_2 \\ T_2 &= -\frac{s_{12}}{s_{11}s_{22} - s_{12}^2}\varepsilon_1 + \frac{s_{11}}{s_{11}s_{22} - s_{12}^2}\varepsilon_2. \end{aligned} \tag{9}$$

Young's moduli and Poisson's ratios in directions 1 and 2 are defined as

$$\begin{aligned} Y_1 &= \frac{1}{s_{11}}, \qquad Y_2 = \frac{1}{s_{22}}, \\ \nu_1 &= -\frac{s_{12}}{s_{11}}, \qquad \nu_2 = -\frac{s_{12}}{s_{22}}. \end{aligned} \tag{10}$$

Also, observe that,

$$\frac{Y_1}{Y_2} = \frac{\nu_1}{\nu_2}. \tag{11}$$

Furthermore, using equations (9) and (10) in (7), the electric displacement along direction 3 due to the in-plane strain along directions 1 and 2 of the piezoelectric film can be expressed as

$$D_3 = \frac{1}{1 - \nu_1\nu_2}\left[(d_{31} + \nu_2 d_{32})Y_1\varepsilon_1 + (d_{32} + \nu_1 d_{31})Y_2\varepsilon_2\right]. \tag{12}$$

Electric displacement is defined as the charge density on the electrode surface. Therefore, the total charge generated by the piezoelectric film Q due to in-plane strains ε_1 and ε_2 of the piezoelectric film is obtained by integrating equation (12) over the surface area of the electrode as

$$Q = \frac{1}{1-\nu_1\nu_2}\left[(d_{31}+\nu_2 d_{32})Y_1\iint \varepsilon_1 dxdy + (d_{32}+\nu_1 d_{31})Y_2\iint \varepsilon_2 dxdy\right]. \tag{13}$$

Finally, assuming the value of strains ε_1 and ε_2 to be averaged over the length l_s and the width w_s of the piezoelectric film, equation (13) can be written as

$$Q = \frac{l_s w_s}{1-\nu_1\nu_2}\left[(d_{31}+\nu_2 d_{32})Y_1\varepsilon_1 + (d_{32}+\nu_1 d_{31})Y_2\varepsilon_2\right]. \tag{14}$$

If the host structure is assumed to be under pure bending, then the longitudinal strain induced in the host structure and thereby in the piezoelectric film, ε_1, can be related to its lateral strain, ε_2, using the Poisson's ratio of the host structure material ν_b, as

$$\varepsilon_2 = -\nu_b\varepsilon_1. \tag{15}$$

Hence, using the above relation, equation (14) can be rewritten as

$$Q = \left[\frac{l_s w_s}{1-\nu_1\nu_2}\left\{(d_{31}+\nu_2 d_{32})Y_1 - (d_{32}+\nu_1 d_{31})Y_2\nu_b\right\}\right]\varepsilon_1. \tag{16}$$

Uniaxially drawn PVDF films can be highly anisotropic. However, the value of Young's modulus for PVDF provided by the manufacturer, Y_s, is non-directional. Therefore, for the present model it is assumed that:

$$\frac{Y_1}{Y_2} = \frac{\nu_1}{\nu_2} = 1.$$

Assuming ν_s to be non-directional Poisson's ratio, equation (16) can be rewritten in the frequency domain as

$$G_2(j\omega) = \frac{Q(j\omega)}{\varepsilon_1(j\omega)} = \frac{l_s w_s Y_s}{1-\nu_s^2}\left\{d_{31}(1-\nu_s\nu_b) - d_{32}(\nu_b-\nu_s)\right\}. \tag{17}$$

Equation (17) gives the charge generated by the sensor per unit longitudinal strain. One of the primary differences between piezoelectric sensors and conventional strain gages is their transverse sensitivity. The transverse sensitivity of a PZT sensor is of the same order as its longitudinal sensitivity, whereas it is an order of magnitude lower for a PVDF sensor than its longitudinal sensitivity. However, for a strain gage, the transverse sensitivity is close to zero and hence it is normally neglected. Therefore, in cases where piezoelectric films are to be used to measure strain, more than one sensor is typically required to isolate the principal strains[2].

Charge sensitivity of the sensor is defined as the charge generated by the sensor per unit applied load. Cascading the transfer functions $G_1(j\omega)$ and $G_2(j\omega)$ yields

$$S_Q(j\omega) = \frac{Q(j\omega)}{F(j\omega)} = \frac{S_C}{\left(\frac{-\omega^2}{\omega_n^2} + j\frac{2\zeta\omega}{\omega_n^2} + 1\right)}\frac{l_s w_s Y_s}{1-\nu_s^2}\left\{d_{31}(1-\nu_s\nu_b) - d_{32}(\nu_b-\nu_s)\right\}. \tag{18}$$

Finally, the static charge sensitivity of the sensor $S_{Q,static}$, can be obtained by setting $\omega = 0$ in the above equation.

2.3. Charge – voltage transfer function

A piezoelectric sensor can be modeled as a capacitor C_s with a finitely large output impedance R_s connected in parallel to a charge source Q. Consider a measurement interface of input impedance Z_M connected in parallel to the piezoelectric sensor. Thus, the transfer function relating the charge input to the voltage output $G_3(j\omega)$ can be given by

$$G_3(j\omega) = \frac{V_O(j\omega)}{Q(j\omega)} = \frac{j\omega}{j\omega C_s + \frac{1}{R_s} + \frac{1}{Z_M}}. \tag{19}$$

Due to the first order nature of the system, the voltage across the terminals of the piezoelectric sensor will always decay to zero. Typically, the resistance due to non-zero conductivity R_s of a piezoelectric material is on the order of several gigaohms at 25°C and it decreases with an increase in temperature. Thus, at room temperature, the decay characteristic of the system is primarily dictated by the input impedance Z_M of the measurement system. For example, a traditional oscilloscope possessing an input impedance of 1 MΩ will yield a time constant on the order of a few milliseconds, thus deterring any reliable quasi-static load measurements. This necessitates Z_M to take the form of an integrator in order to increase the time constant of the piezoelectric sensor. An integrator can be physically realized through an ideal charge amplifier as shown in the Figure 2(a).

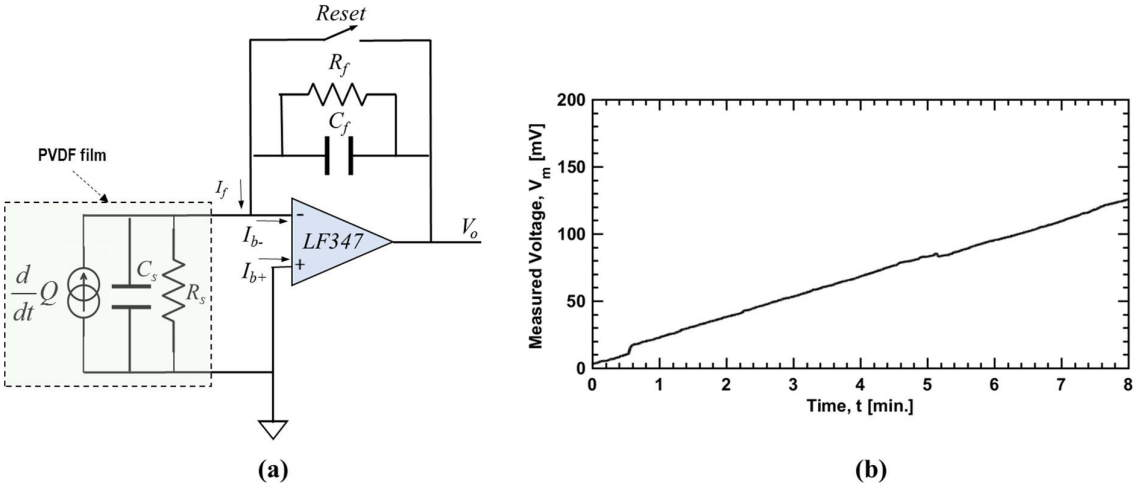

Figure 2. (a) Equivalent circuit model of PVDF sensor connected to a charge amplifier, (b) voltage measured over time due to input bias current for the operational amplifier shown on the left.

Given the input resistance of the operational amplifier R_o, feedback capacitance C_f, and feedback resistance R_f and neglecting other stray capacitances and resistances in the system, equation (19) can be rewritten as

$$G_3(j\omega) = \frac{V_O(j\omega)}{Q(j\omega)} = \frac{j\omega}{j\omega(C_s + C_f) + \frac{1}{R_s} + \frac{1}{R_f} + \frac{1}{R_o}} = \frac{\left(\frac{j\omega}{C_{eq}}\right)}{j\omega + \frac{1}{R_{eq}C_{eq}}} \tag{20}$$

where R_{eq} and C_{eq} are the equivalent resistance and capacitance of the overall electrical system. The circuit sensitivity is thus defined by the reciprocal of the equivalent capacitance and the circuit time constant given by $\tau = R_{eq}C_{eq}$. Note that in

practice, the time constant of this first order electrical system is largely dependent on the values of its feedback resistance and capacitance.

Now the overall transfer function of the PVDF sensor system $G(j\omega)$ can be derived by using equations (18) and (20):

$$G(j\omega) = \frac{V_o(j\omega)}{F(j\omega)} = \frac{S_Q\left(\frac{j\omega}{C_{eq}}\right)}{j\omega + \frac{1}{R_{eq}C_{eq}}}. \tag{21}$$

Thus, neglecting second order effects, the response of the above system when subjected to a step input of magnitude F can be expressed as

$$V_o(t) = \left\{\frac{S_{Q,static}}{C_{eq}} e^{-\left(\frac{t}{R_{eq}C_{eq}}\right)}\right\} F. \tag{22}$$

Equation (22) suggests that reliable quasi static measurements can be conducted if the equivalent time constant of the sensor system is large. Finally, if $\tau \to \infty$, the quasi-static sensitivity of the sensor κ is then obtained by

$$\kappa = \frac{V_o}{F} = \frac{S_{Q,static}}{C_{eq}}. \tag{23}$$

For most measurement systems, the value of the feedback capacitance C_f is prescribed by the desired circuit sensitivity, but the value of feedback resistance R_f is an outcome of conflicting requirements. It should be sufficiently large to provide a long time constant and also sufficiently small to overpower drift and lower resistance noise. For an ideal operational amplifier with no input bias currents, the value of R_f can just be the insulation resistance of the feedback capacitor, which is typically on the order of 10^{12} Ω. This satisfies the need for a large time constant with low resistance noise. But due to the finite resistance of the operational amplifier at the input stage, leakage currents can flow through the feedback capacitor causing a drift in the output voltage V_d. This drifting output is not a function of the applied load and as such, it will continue in either direction until the operational amplifier is saturated. Apart from the drift error, an operational amplifier can also have a constant offset voltage error V_{off}. Typically, the influence of V_{off} is negligible compared to V_d. Thus, the total error in output voltage in the time domain V_e due to input bias current at the inverting terminal I_{b-} in a charge amplifier of feedback capacitance C_f and V_{off} can be expressed as

$$V_e(t) = \frac{I_{b-}}{C_f} t + V_{off}. \tag{24}$$

For a charge amplifier circuit constructed with an LF347 quad operational amplifier and a feedback capacitance C_f = 100 nF with insulation resistance $R_f = 10^{12}$ Ω, the error in output voltage over time is shown Figure 2(a). For the LF347, with a 5 V supply voltage, the input bias current is computed to be 26 pA at room temperature.

3. PROPOSED DRIFT COMPENSATION METHOD

Various techniques for automated drift compensation have been proposed in the literature. Most of these solutions were developed exclusively for specific measurement applications. In this paper, we propose an analog implementation of drift compensation particularly for near DC measurements using piezoelectric sensors. The basic principle of this technique is the real time error cancelation through construction of a dummy charge amplifier on the same quad operational amplifier with a feedback capacitance equal to the active charge amplifier as shown in the Figure 3(a).

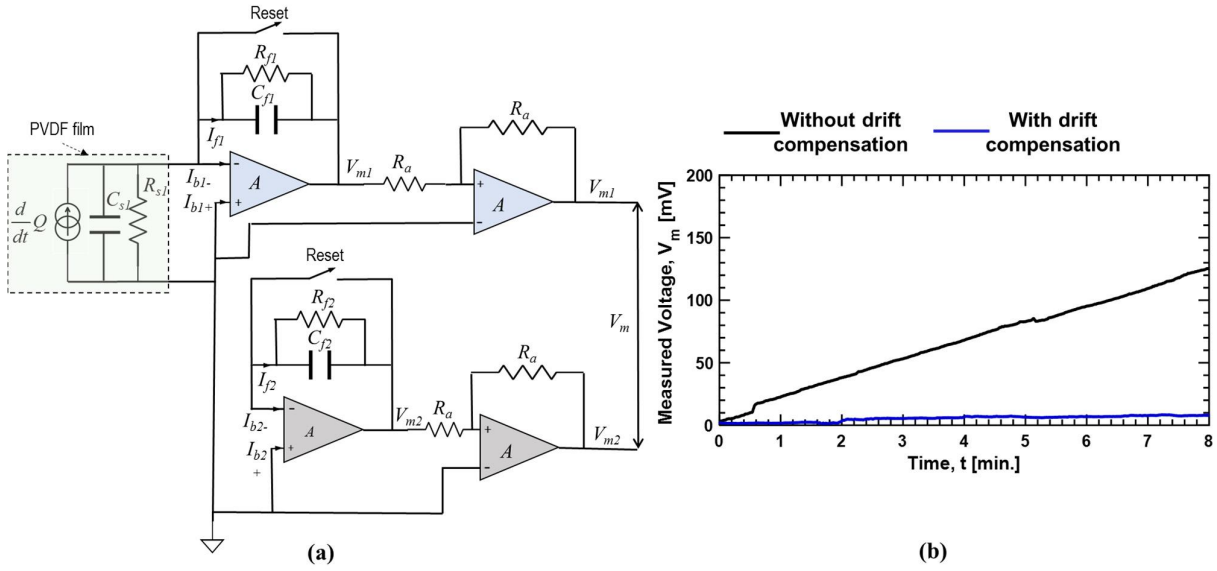

Figure 3.(a) Proposed drift compensation circuit, (b) comparison of measured voltage between conventional charge amplifier vs proposed drift compensation circuit.

The voltages measured from the active charge amplifier V_{m1} and dummy charge amplifier V_{m2} at constant temperature with respect to the common ground are given by

$$V_{m1}(t) = V_o(t) + V_{e1}(t) = V_o(t) + \frac{I_{b1-}}{C_{f1}}t + V_{off1} + V_{IC1}$$
$$V_{m2}(t) = V_{e2}(t) = \frac{I_{b2-}}{C_{f2}}t + V_{off2} + V_{IC2} \tag{25}$$

where V_{IC} is the error in the measured voltage due to residual charges in the feedback capacitors. The subscripts 1 and 2 in the above equations refer to the values in the active circuit and dummy circuit, respectively. The output voltages from the charge amplification stage are then fed into unity gain voltage follower stages (buffer circuits) in order to eliminate loading effects of the data acquisition system. The voltage thus measured between the terminals of the voltage followers can be expressed as

$$V_m(t) = V_{m1}(t) - V_{m2}(t) = V_o(t) + \left(\frac{I_{b1-}}{C_{f1}}t - \frac{I_{b2-}}{C_{f2}}t\right) + \left(V_{off1} - V_{off2}\right) + \left(V_{IC1} - V_{IC2}\right). \tag{26}$$

Errors due to residual charges in the feedback capacitors at the start of the measurement can be eliminated by implementing reset switches across the feedback capacitors, which forces the output voltage to zero prior to the start of measurement. Assuming the values of feedback capacitances, bias currents at the inverting terminal, and offset voltages of both the operational amplifiers to be equal and independent, the voltage due to the piezoelectric charge input is completely recovered. However, in practice, there is expected to be some variation in these parameters due to manufacturing inaccuracies[18]. Nevertheless, the error in measured voltage is found to be minimal compared to a single charge amplifier implementation as shown in Figure 3(b). For maximum error minimization the bias currents and offset voltages are required to be equal. It is possible that these requirements can be met with operational amplifiers fabricated on the same chip[18], but it is not necessary to construct the unity buffer circuit from the same chip.

4. EXPERIMENTAL INVESTIGATION

Experimental testing was conducted in order to demonstrate the ability of the drift compensation circuit to provide long near DC force measurements and also to validate the model presented in section 3. The testing also demonstrates the suitability of PVDF film as a highly sensitive active material for low force measurements.

4.1. Experimental Setup and Methods

In order to test the drift compensation circuit presented above with a piezoelectric sensor, a PVDF film was bonded at the center of a Polymethyl methacrylate (Plexiglass PMMA) sheet using a thin layer of cyanoacrylate glue as shown in the inset of Figure 4. The PVDF film was manufactured by TE Connectivity Inc., model LDT1-028K which is laminated between thin sheets of Mylar. The PMMA sheet was then set up in a simply supported three-point bend configuration on an MTS Criterion® load frame with the load applied along its mid-plane as shown in Figure 4. The applied load was measured by an MTS load cell (LPS 504) with a sensitivity of 2.15 mV/N. The room temperature was measured and assumed to constant at 25°C throughout the experiment. Typical material properties of PMMA at room temperature were assumed for the host structure. The piezoelectric constants and the Young's modulus of the PVDF film were provided by the manufacturer[20]. The Poisson's ratio of the PVDF film[7] is assumed to be equal to 0.39. The capacitance of the film was measured using a digital multimeter prior to the experiment and the charge amplifier was constructed using LF347 quad operational amplifiers as shown in Figure 3(a). The geometric, material, and electrical parameters are given in Table 1. The data was originally recorded at 1 kHz using an NI cDAQ and then downsampled to 10 Hz using an array averaging technique within NI Labview for storing and analyzing long sample time records of the measured voltage.

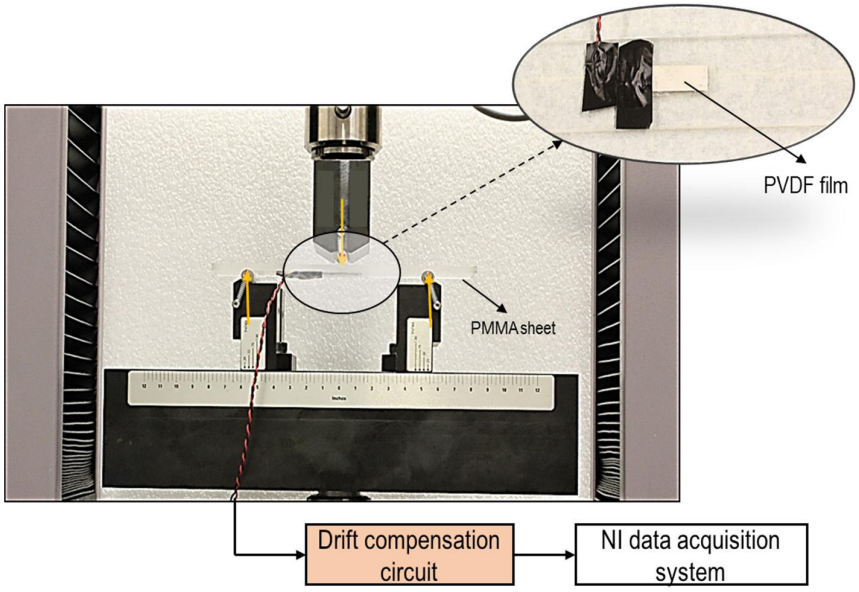

Figure 4. Experimental setup of the PVDF force sensor mounted in a load frame.

Two sets of experiments were conducted with three loading cases, F = 10, 20, and 30 N for each set. Prior to each measurement, the load and the circuit were reset in order to force the measured voltage to zero. Since an ideal step input was not possible with the current setup, the load was ramped to the desired value using the load frame controller. The measurement for each case was conducted for 500 seconds.

Table 1. PVDF force sensor properties. For the geometric parameters, the subscripts *b* and *s* refer to the host structure and the PVDF film, respectively.

Geometric parameters		**Material properties**	
Length x width x thickness of the host structure, l_b x w_b x t_b	135 x 43 x 5 [mm]	Young's modulus of the host structure, E_b	3.6 [GPa]
Length x width x thickness of the sensor, l_s x w_s x t_s	30 x 12 x 0.028 [mm]	Poisson's ratio of the host structure, v_b	0.35
Electrical parameters		Young's modulus of PVDF film, Y_s	2.4 [GPa]
		Poisson's ratio of PVDF film, v_s	0.39
Feedback capacitance, C_f	100 [nF]	Piezoelectric charge coefficient of PVDF film in direction 1, d_{31}	23 [pC N^{-1}]
Insulation resistance of the feedback capacitance, R_f	10^{12} [Ω]	Piezoelectric charge coefficient of PVDF film in direction 2, d_{32}	3 [pC N^{-1}]
PVDF film capacitance, C_s	1.44 [nF]	Piezoelectric charge coefficient of PVDF film in direction 3, d_{33}	-33 [pC N^{-1}]
PVDF film output resistance, R_s	10^{12} [Ω]	Dielectric constant of PVDF film in direction 3, K_{33}	113 [pF m^{-1}]
Operational amplifier input resistance, R_o	10^{12} [Ω]	Pyroelectric constant of PVDF film, p	40 [μC $m^{-2}K$]

4.2. Discussion of Results

The first set of measurements was taken with the voltage measured from the active charge amplifier with respect to common ground, i.e. V_{m1}. In this set, the output is expected to drift until saturation after the application of load, since the saturation time for the operational amplifier is much lower than the time constant of the electrical circuit. The second set of measurements was taken with the voltage measured between the two charge amplifiers, i.e. V_m as shown in Figure 3(a). The error voltage over time is computed analytically using equation (24) and is then subtracted from the measured voltage of the first set of measurements. Thus, the resulting voltage is the maximum reduction in error that could be obtained from an ideal drift compensation circuit. Comparison of this resulting voltage with the voltage measured from the actual drift compensation circuit demonstrates the fidelity of the proposed technique. Figure 5(a) shows the difference between the measured voltage with ideal drift subtracted and the voltage measured from the real time drift compensation circuit. The difference stays within ±10 mV (or 5%) over the entire measurement period and does not tend to change with respect to applied load. It can be extrapolated to compute that the measured value stays within 5% over a half hour measurement. The lower cutoff frequency of this system is calculated to be 0.005 mHz, thus enabling reliable near DC force measurements. Although the model suggests that the high frequency performance is limited only by the natural frequency of the structure, this has not yet been experimentally verified.

It should be noted that even though the error due to voltage drift has been eliminated, this does not prevent the operational amplifier from saturating. For the current system at room temperature, the operational amplifier saturates in 320 minutes. Another limitation of this system is the requirement of a constant temperature environment. As such, the pyroelectric nature of PVDF deters its application as a sensor in highly fluctuating environments without appropriate temperature compensation. Also, as the temperature increases, the output impedance of the PVDF decreases and the input bias current of the operational amplifier increases. This potentially affects the available measurement time before the operational amplifier saturates. This technique does not compensate for other extraneous errors during measurement, such as creep, cross sensitivity to humidity, or electromagnetic interference. Finally, the performance of the system is comparable to expensive 20 fA ultra-low bias current operational amplifiers. Nevertheless, the proposed technique can also be applied in conjunction with those operational amplifiers, as well as with conventional charge readout algorithms in order to further minimize the integration error.

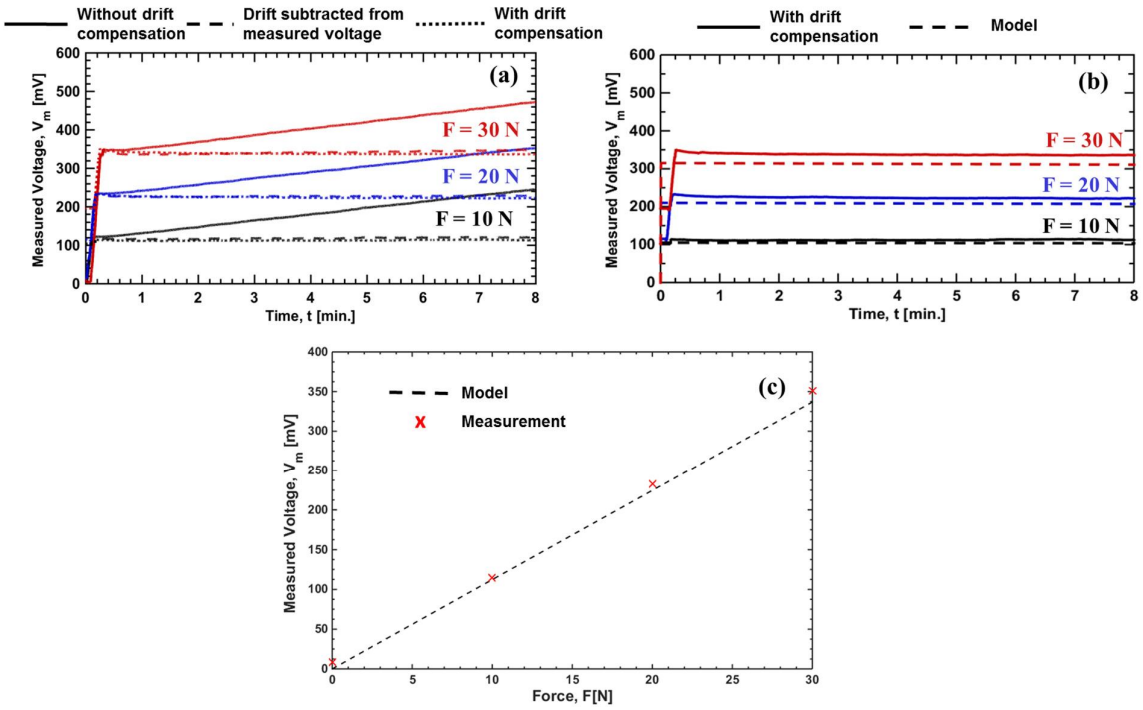

Figure 5. (a) Measured voltages comparing ideal drift compensation circuit and actual circuit, (b) Comparison of measured voltage from actual drift compensated circuit vs model, (c) Sensitivity plot of the developed piezoelectric sensor vs model.

The second objective of the testing is to validate the model proposed in section 2. Using the geometric, material, and electrical parameters given in Table (1), the response of the system when subjected to a step force input of F = 10, 20, and 30 N computed using equation (22) is shown in Figure 5(b). It can be seen that within the loading range tested, the two sets of results are in good agreement. The error between the responses is computed to be within 10 mV (or 5%) over the entire measurement period. The developed PVDF sensor was calibrated against the load cell by relating the maximum value of measured voltage in each load case (Figure 5(c)). The sensitivity thus obtained by linear regression of the corresponding data points is 11.46 mV/N. This value is slightly higher than the model prediction of 10.5 mV/N. This could be attributed to overshoot in the actual system due to second order effects and non-directional material assumption of the sensor model. Finally, the full-scale range of the system is limited electrically for a 5 V supply voltage to be 430 N.

5. CONCLUDING REMARKS

This work developed a system-based model relating the input force and output voltage from a PVDF sensor interfaced with a drift compensated charge amplifier. The sensor exhibits excellent linearity within the loading range. The sensitivity and response to a step input is found to agree well with measurements with error less than 5%. The model could be further improved upon availability of directional material properties of the PVDF sensor. This article also described and demonstrated low cost, straightforward, analog implementation of a drift compensation technique for long quasi-static force measurements using piezoelectric sensors. It was found that the measured value stayed within 5% for a half-hour measurement, thus enabling reliable near DC measurements. In the future, this work will be expanded by experimentally characterizing the dynamic performance of the system, studying the effects of ratio of feedback capacitance to piezoelectric capacitance, and implementing temperature compensation. The methodology can then be directed towards other potential application areas, such as pressure and torque sensing.

Acknowledgement

Financial support was provided by the member organizations of the Smart Vehicle Concepts Center, a National Science Foundation Industry-University Cooperative Research Center (www.smartvehiclecenter.org).

REFERENCES

[1] Zhang H., Galea S.C., Chiu W.K., and Lam Y.C. "An investigation of thin PVDF films as fluctuating-strain-measuring and damage-monitoring devices", *Smart Materials and Structures* 2, no. 4: 208 (1993).
[2] Sirohi J., and Chopra I. "Fundamental understanding of piezoelectric strain sensors", *Journal of Intelligent Material Systems and Structures* 11, no. 4: 246-257 (2000).
[3] Lee, C.K. and O'Sullivan, T.C. "Piezoelectric strain rate gages", *The Journal of the Acoustical Society of America, 90(2)*: 945-953 (1991).
[4] Debashis Satpathi J.P., Victor M.L., Yang H.Y., and Shih C.C. "Development of a PVDF film sensor for infrastructure monitoring", *Proceedings of SPIE, Smart Structures and Materials 1999: Smart Systems for Bridges, Structures, and Highways*, Vol. 3671, Newport Beach, CA. (May 18, 1999).
[5] Romero J.G., García-Torales G., Rosas G., Ocaña J.L., and Flores J.L. "Characterization of mechanical shock waves in aluminum 6061-T6 using a high power laser pulse", *Proceedings of SPIE. Infrared Remote Sensing and Instrumentation XXIV*, Vol. 99730, San Diego, CA. (September 14, 2016).
[6] Headings L.M., Kotian K., and Dapino M.J. "Speed of sound measurement in solids using polyvinylidene fluoride (PVDF) sensor", *ASME Conference on Smart Materials, Adaptive Structures and Intelligent Systems*, American Society of Mechanical Engineers, pp. V001T04A012-V001T04A012, Snowbird, UT. (September 16-18, 2013).
[7] Xu J., Dapino M.J., Gallego-Perez D., and Hansford D. "Microphone based on polyvinylidene fluoride (PVDF) micro-pillars and patterned electrodes", *Sensors and Actuators A: Physical*. 153(1): 24-32 (2009).
[8] Ngalamou L., Noury N., Chamberod E., and Benech P. "Analysis of the sensitivity and the temperature influence of a static force sensor based on a PVDF resonator", *Sensors and Actuators A: Physical* 57, no. 3: 173-177 (1996).
[9] Motoo K., Fumihito A., and Toshio F. "Piezoelectric vibration-type tactile sensor using elasticity and viscosity change of structure", *IEEE Sensors Journal* 7, no. 7: 1044-1051 (2007).
[10] Li C., Wu P.M., Shutter A.L., and Narayan R.K. "Dual-mode operation of flexible piezoelectric polymer diaphragm for intracranial pressure measurement", *Applied Physics Letters* 96, no. 5: 053502 (2010).
[11] Gehin, C., Barthod C., and Teisseyre Y. "Design and characterisation of a new force resonant sensor", *Sensors and Actuators A: Physical*, 84.1-2: 65-69 (2000).
[12] Barthod, C., Teisseyre, Y., Géhin, C., and Gautier, G. "Resonant force sensor using a PLL electronic", *Sensors and Actuators A: Physical*, 104(2): 143-150 (2003).
[13] Li F., and Jiang Z. "Development of a piezo-cantilever transducer and measuring method for evaluation of a temperature-sensitive polymer gel membrane", *Smart Materials and Structures* 16, no. 3: 858 (2007).
[14] Castellini P., Montanini R., and Revel G. "A new sensor for static and dynamic force measurement", *Proceedings of SPIE. Photo-Optical Instrumentation Engineering*. Vol. 4798, San Diego, CA (December 27, 2002)
[15] Lin C.H., Tsai M.C., and Hsiao S.W. "Static force measurement for automation assembly systems", *Sensors and Actuators A: Physical* 187: 147-153 (2012).
[16] Lord M., and David M.S. "Static response of a simple piezoelectric load cell", *Medical Engineering and Physics* 5.2: 162-164 (1983).
[17] Park K.T., Klafter R.D., and Bloomfield P.E. "A charge readout algorithm for piezoelectric force transducers", *Sixth IEEE International Symposium on Applications of Ferroelectrics*. San Jose, CA. (June 8-11, 1986).
[18] Brandolini A., Gandelli A., and Ottoboni R. "Silicon strategies to increase performance of piezoelectric sensors", *IEEE Instrumentation and Measurement Technology Conference. IEEE, Hamaratsu, Japan.* (May 10, 1994).
[19] Rosenbaum K.A., Pekarek S.D., Baudendistal T., and Jordan B. "A low-cost force sensor for electromechanical actuation systems", *Vehicle Power and Propulsion Conference, 2007. VPPC IEEE,* Arlington, TX. (September 9, 2007).
[20] "Piezo Film Sensors Technical Manual", Measurement Specialties Inc., Norristown, PA. (1999).